Asian Journal of Chemistry; Vol. 35, No. 8 (2023), 1869-1878

ASIAN JOURNAL OF CHEMISTRY

https://doi.org/10.14233/ajchem.2023.28042

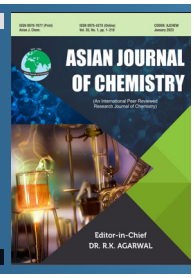

Enhanced Anticorrosive Properties of Silane Functionalized Polybenzoxazine @CeO_2 Nanocomposites with Polyurethane Coatings on Mild Steel

N. VALARMATHI[1,*], M. SIVARAJU[2,*] and P. SHANMUGASUNDARAM[2]

[1]Department of Chemistry, Vivekanandha College of Arts and Sciences for Women (A), Elayampalayam, Tiruchengode-637205, India
[2]Department of Chemistry, Thiruvalluvar Government Arts College, Rasipuram-637401, India

*Corresponding author: E-mail: msivarajuchemistry@gmail.com; valarkumar84@gmail.com

Received: 20 May 2023; *Accepted*: 16 June 2023; *Published online*: 31 July 2023; AJC-21319

In this study, the durability of polyurethane adhesives are successfully developed using silane-functionalized polybenzoxazine@CeO_2 nanocomposites. The electrochemical measurements were used to investigate the mechanical strength of polybenzoxazine nanocomposite with polyurethane materials. The superior results in the process of passivation film that also controlled the dissolution of metal have been characterized by UV-visible, XRD, SEM/EDX, FT IR, TGA-DTA-DSC, micro hardness, gel absorption and water absorption analyses. The mechanical performance of the coated surface that supported up the electrochemical investigations was enhanced by the incorporation of silane functionalized polybenzoxazine@CeO_2 nanocomposites with polyurethane. The use of ploy urthane in the TGA process increases the cross-linked density of the coating, resulting in high thermal stability. As a result of their superior anticorrosive property, the proposed polybenzoxazine@CeO_2 nanocomposites with polyurethane films offer the openings for the development of unique, state-of-the-art anticorrosive adhesives across a wide range of sectors.

Keywords: CeO_2 nanoparticles, Silane, Polybenzoxazine, Polyurethane, Dip-coatings, Corrosion protection.

INTRODUCTION

Polymer nanocomposites have emerged as one of the most studied and commercialized areas of nanotechnology because of their impressive effectiveness and adaptability. Improved mechanical, thermal, optical and barrier properties are regularly observed when comparing these materials to standard composites and pure polymers [1-3]. The incorporation of nanostructured materials not only restores the adhesive's effectiveness on both mechanical and physical properties, but also provides numerous cognitive functions, including super hydrophobicity, electroactivity, self-healing properties, and other characteristics [4,5]. Therefore, it is possible that defects in the adhesives and a decrease in their durability could result from insensitivity between polymer matrix and nanostructure materials. Particle agglomeration is triggered by hydrophobic attraction clusters between the nanoparticles due to the presence of surface hydroxyl groups; this phenomenon can be studied as a new polymeric coating is developing. Physical and chemical processes have had significant impacts in describing this problem [6-8].

One of the inorganic nanocomposite coating material is CeO_2 nanoparticles which have both cytotoxic and cytoprotective effects. The best applications of ceria is for polishing especially chemical-mechanical planarization, automotive exhaust treatment, solar cells, catalytic materials, automotive exhaust treatment, alternative additives in solvent based alkyd coatings in order to improve anti-aging and anticorrosive agent, *etc.* [9-11]. The interactions of a nanoparticle system with its microenvironment need to be considered while designing effective nanocarriers, which is also important to the polymeric nanocarriers [12-15].

Polybenzoxazines have the potential to relate as corrosive environment protective layer in the past 10 years due to their unique properties, such as limited water uptake, low surface weak strength, almost negligible deformation and extraordinary piezoelectric dwellings [16-18]. Parallel to this, a new silane functionalized polybenzoxazine precursor (TEOS-BZ) is developed and its polymerization spraying (TEOS-PBZ) using dipped protective layer and the conventional thermal curing procedure, which exhibited the real resistance to oxidation for

steels [19]. It has also been suggested that due to the presence of the Si-O-Si bond and polybenzoxazine molecules within the TEOS-PBZ matrix, as well as its potent hydrophobic character and platform adherence, enhanced the TEOS-PBZ coating corrosion prevention. Additionally, during the dipped film formation, the energetic hydroxy structures of TEOS-BZ might undergo hydrolysis and transform into silanol groups (SiOH), allowing them to easily interact with the hydroxy groups that are present of SiO_2 nanoparticles without forming a cohesive link [20]. It is possible to increase the corrosion protection of TEOS-PBZ/CeO_2 nanocomposites with polyurethane coatings by integrating CeO_2 nanoparticles into the covering.

The main objective of present work is to develop coatings composed of silane-functionalized polybenzoxazine nanoparticles encapsulated in CeO_2 (PBZ-TEOS@CeO_2 nanocomposites) that can be dissociated in polyurethane. In 3.5% NaCl electrolyte solution, the corrosion performance of polyurethane, polyurethane-silane functionalized polybenzoxazine (TEOS-PBZ), polyurethane-cerium oxide (PU-CeO_2) and polyurethane-tetraethoxy-silane-polybenzoxazine-cerium oxide (PU/TEOS-PBZ@CeO_2) coatings was evaluated using electrochemical impedance spectroscopy (EIS), Tafel polarization (TP) and the ground morphological studies had been executed using SEM/EDX techniques. A new amide bond formation may additionally need to decorate the dispersibility in the polymer matrixes. To the best of our knowledge, TEOS-PBz/PU@CeO_2 nanocomposite coating has not been established to be the result of the functionalization of silane supported polybenzoxazine and its scattering in polyurethane coating.

EXPERIMENTAL

The chemicals such as cerium(III) nitrate hexahydrate ($Ce(NO_3)_3{\cdot}6H_2O$), potassium carbonate, 4-hydroxybenzaldehyde, triethoxysilyl propylamine (TEOS), paraformaldehyde 1,4-dioxane, ethyl acetate, sodium hydroxide, anhydrous sodium sulfate, polyurethane, *etc*. were procured from Sigma-Aldrich, Spectrochem and HIMEDIA Lab Pvt. Ltd., India. All the chemicals and solvents were of AR grade and used without any additional purification.

Synthesis of monomer: The 4-hydroxybenzaldehyde, triethoxysilyl propylamine and paraformaldehyde dissolved in chloroform were mixed in a round-bottomed flask and fixed water condenser in 16 h. The completion of the reaction was monitored by TLC and then the reaction mixture was extracted with ethyl acetate washed with 0.1 N NaOH, water and brine solution. The organic layer was separated and dried over anhydrous sodium sulfate solution [21,22]. Finally, the product was collected as pale yellow oil, which was characterized by UV-Visible, FT-IR spectroscopy and NMR spectral techniques.

Synthesis of CeO_2 nanoparticles: The co-precipitation method was applied to synthesize cerium oxide nanoparticles by using cerium nitrate (0.434 g) dissolved in 50 mL distilled water (50 mL) followed by the addition of 20 mL potassium carbonate (0.086 g) in a dropwise manner. Further, the mixture was diluted to 100 mL using distilled water and stirred magnetically for 0.5 h. Then adjust the solution to pH 6 and continued to stir for 1 h. The prepared powder (CeO_2 NPs) was centrifuged at normal rpm and calcined for 3 h at 600 ºC [23,24].

Dip plating method: The derived monomer dissolved in 1,4-dioxane and then 5% of nano-CeO_2 was incorporated. Polyurethane adhesive in toluene was added to the reaction mixture. Three specific silane functionalized polybenzoxazines and polyurethane combinations (100:60, 100:80, 100:100) along with 5% nano-CeO_2 was prepared. The sanitized mild steel (MS) was cleaned with emery paper to develop adhesion. The MS was cleaned by being submerged in a TEOS-PBZ:PU: nano-CeO_2 solution for 1 min before being removed systemati-cally [25]. Finally, after 3 h of heating and treating at 200 ºC throughout the furnace, the mild steel inside has been effectively heated and treated. The electrochemical impedance experiments have also been performed on the dipped mild steel. The chemical synthetic route of silane functionalized polybenzoxazine CeO_2 nanocomposites with polyurethane is shown in **Scheme-I**. ^{1}H NMR ($CDCl_3$, δ ppm): 0.580 (2H, t, CH_2 Si O), 1.143 (-CH_3 appear triplet), 1.548-1.530 (m, CH_2CH_3), 2.508 (2H, t, NCH_2), 2.651 (N-CH_2-C), 3.690 (6H, q, -OCH_2), 3.362 (2H, d, $ArCH_2CH{=}CH_2$), 3.750 (6H, q, Si-O-CH_2), 4.034 (2H, s, Ar-CH_2-N), 4.966 (2H, s, OCH_2N), 6.883 (1H, s, Ar-H), 6.903 (1H, t, Ar-H), 7.623-7.714 (1H, d, ArH), 9.801 (1H, s, CHO).

Electrochemical analysis: Three electrodes system was applied in the electrochemical measurements for measured with the coated sample acted as the working electrode, as Ag/AgCl electrode and saturated KCl electrode were used as the reference electrode and a stainless steel cylinder as counter electrode. The area of the working electrode was kept at 14 cm^2. At ambient temperature, the corrosive medium of 3.5% NaCl aqueous solutions were performed in the all tests. To ensure the steadystate prior to the measurements of the samples were immersed for 0.5 h and then the measurements were conducted at least three times. In the electrochemical impedance spectroscopy (EIS) measurements, a sinusoidal AC perturbation of 10 mV amplitude coupled with the open circuit potential was used in metal-coating system. The EIS analysis was conducted in the frequency range from 100 kHz to 0.01 Hz by using Z view software [26,27].

RESULTS AND DISCUSSION

UV-visible studies: The electronic changes inside the model give rise to absorption in the near brilliant region. Fig. 1a shows the UV-Vis spectra of both as-prepared and tempered CeO_2 nanoparticles. For as-synthesized CeO_2 nanoparticles, the blue shift is readily apparent due to the presence of a significant absorption band at low frequency close to 270 nm. It shows that the maintenance positions vary with the shapes and sizes of CeO_2. In addition, Fig. 1b demonstrates that the maximum absorbance of benzoxazine monomer was determined to be 382 nm.

A time-dependent UV-vis spectrum for silane-functionalized polybenzoxazine@CeO_2 nanocomposites in polyurethane at room temperature is shown in Fig. 1c, where two retention peaks have appeared at 331 and 288 nm, corresponding to the π-π* transition of the C=C paraformaldehyde moiety and the δ-δ* transition of polybenzoxazine ring, respectively. With

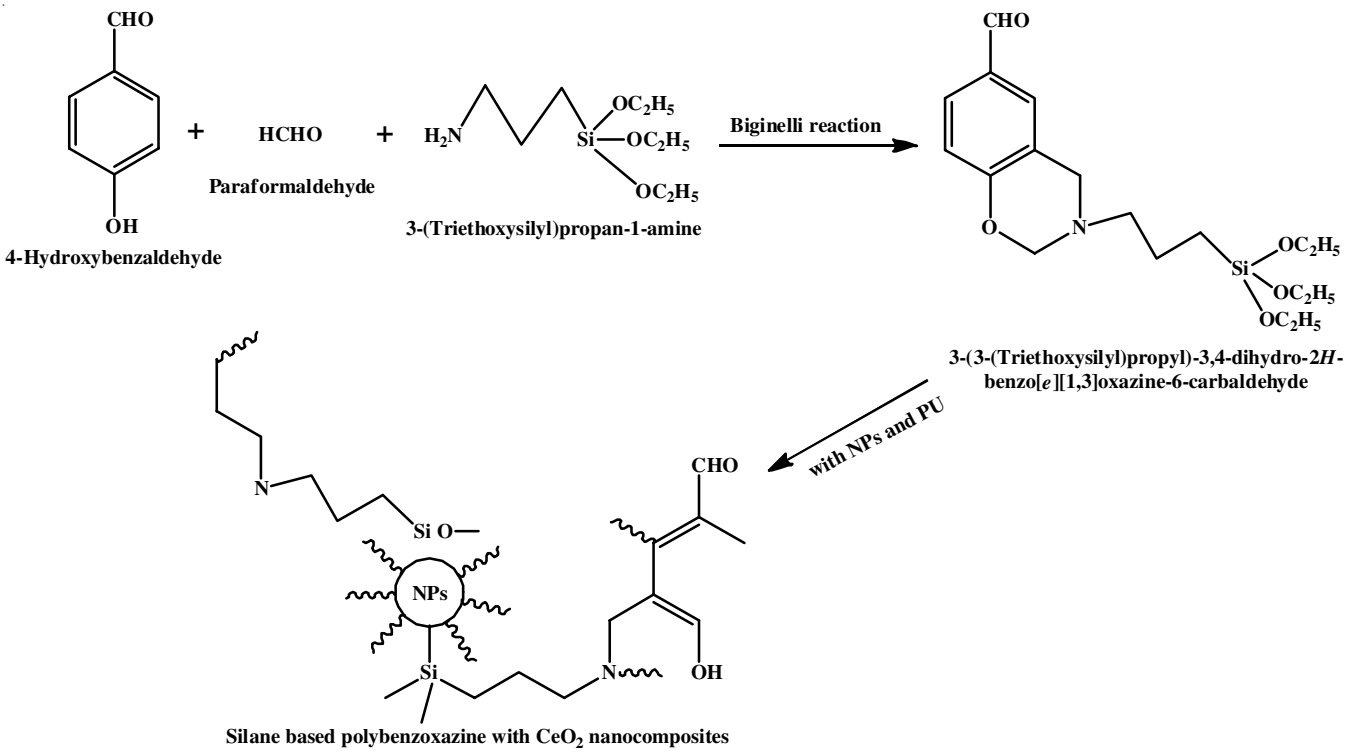

Scheme-I: Synthesis and formation of silane functionalized polybenzoxazine CeO_2 nanocomposites with polyurethane

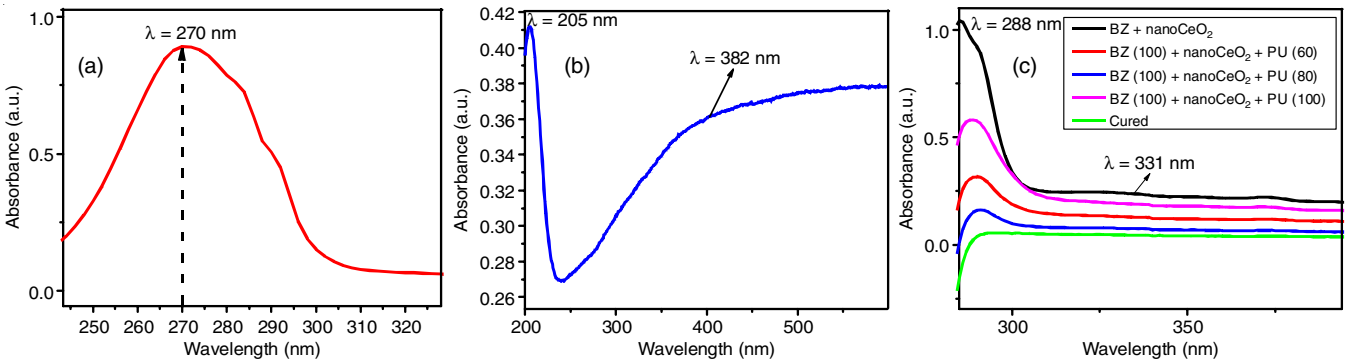

Fig. 1. UV-visible absorption spectroscopy of (a) CeO_2 NPs (b) benzoxazine monomer (c) silane functionalized polybenzoxazine CeO_2 nanocomposites with polyurethane

increasing preparation time, the silane-functionalized polybenzoxazine-CeO_2 nanocomposites exhibit a decrease in the peak at 331 nm and an increase in the strength at 288 nm. This behaviour clearly shown that polybenzoxazine possesses an induced moiety (paraformaldehyde), which can be gone through to a photodimerization response when its ability to absorb to light illumination is increased. The aforementioned findings suggested that a union of polybenzoxazines is necessary and effective [28,29].

FTIR studies: The FTIR spectra of CeO_2, silane functionalized polybenzoxazine@CeO_2 nanocomposites with polyurethane are shown in Fig. 2a-b. The Ce-O-Ce vibration is addressed by a strong band at 786 cm^{-1}, which confirmed the presence of CeO_2 nanoparticles, whereas the strong and broad peak at 3385.90 cm^{-1} is attributed to the increased vibration of the hydroxyl group. In polybenzoxazine, the benzoxazine moiety at 1647 cm^{-1} and also confirmed the presence of the C=O, N-H and C=C vibrations, thus, indicating the presence of fragrant amino groups in polybenzoxazine. The broad peak at 3500-3000 cm^{-1} is attributed due to the O-H and N-H strecting modes because of functionalization of CeO_2 nanoparticles by polybenzoxazine [30]. In silane functionalized polybenzoxazine@CeO_2 nanocomposites, benzoxazines attribute both CeO_2 and TEOS-PBZ, suggested that CeO_2 nanoparticles are inserted in the polybenzoxazine containing polyurethane.

X-ray diffraction studies: Fig. 3a-b illustrates the XRD investigation of CeO_2 and silane functionalized polybenzoxazine@CeO_2 nanocomposites with polyurethane. The diffraction peaks at 28.6º, 33.2º, 47.5º, 56.4º, 59.1º, 69.4º, 77.0º and 79.1º, correspond to (111), (200), (220), (311), (222), (400), (331) and (420) of CeO_2 and silane functionalized polybenzoxazine@CeO_2 nanocomposites containing polyurethane coating are in great concurrence with cubic fluorite structure CeO_2 (JCPDS card No. 340382). The XRD analysis confirmd the

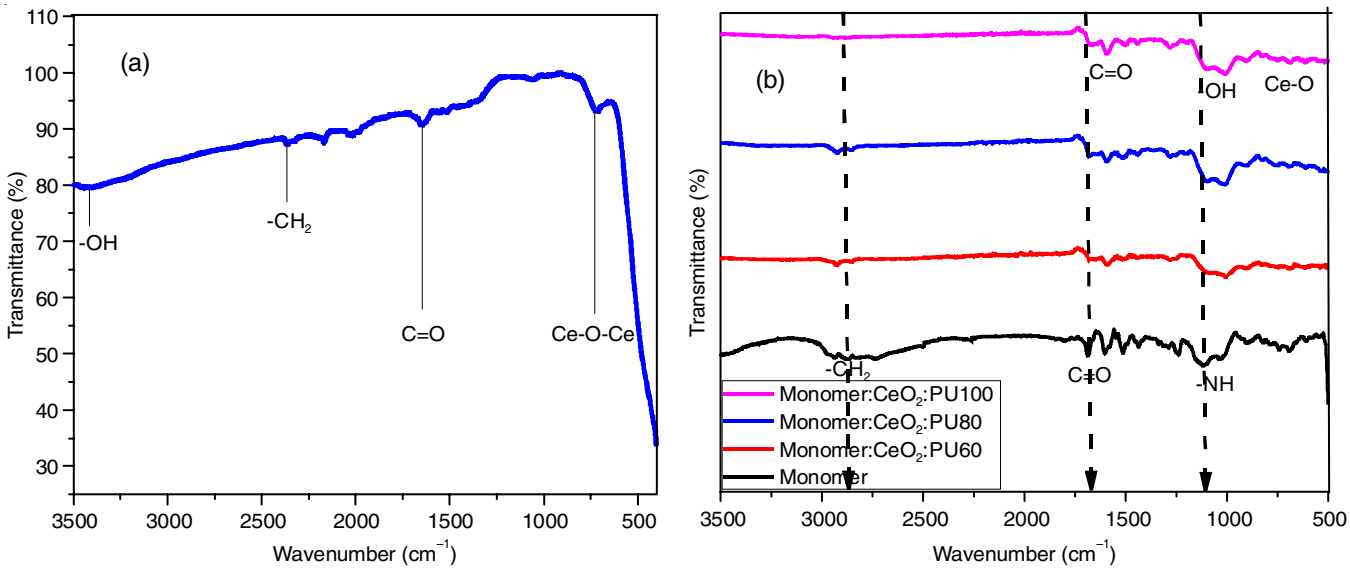

Fig. 2. Vibrational spectroscopy of (a) CeO_2 NPs (b) silane functionalized polybenzoxazine @ CeO_2 NCs with PU for corrosion protection on mild steel in 3.5% NaCl for immersion of 5 days

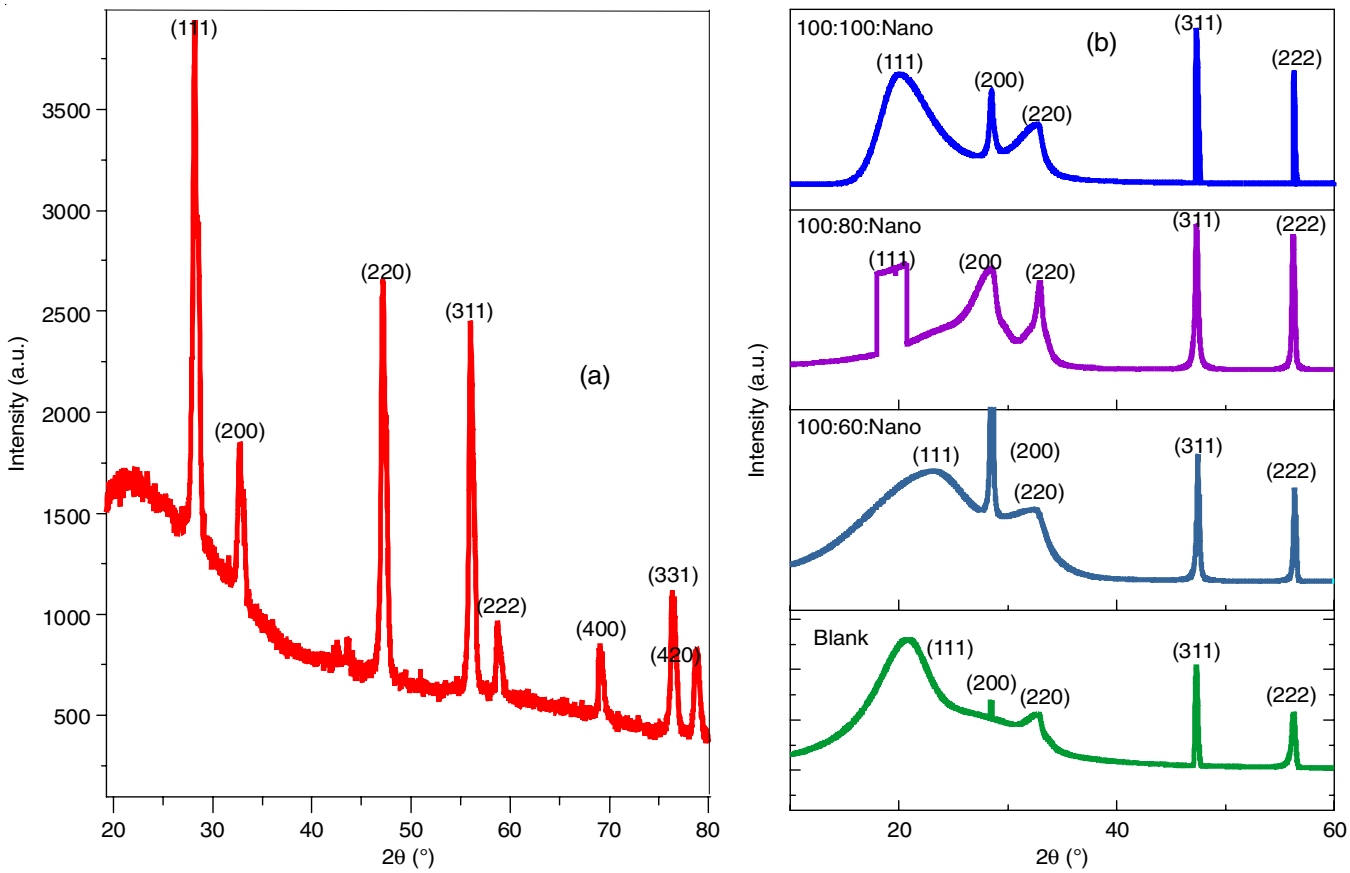

Fig. 3. XRD pattern of (a) CeO_2 NPs (b) XRD design secured for the various combination of PBZ: PU: % CeO_2 nanocomposite coated with mild steel soaked in 3.5% NaCl for 5 days

encapsulation of TEOS-PBZ over the CeO_2 surface. However, due to silane functionalized polybenzoxazine@CeO_2 nanocomposites with polyurethane, the characteristic peak behaves almost identically to CeO_2 with low force and no shift was observed. The diminished force without the distinctive change in peaks demonstrated that the design of CeO_2 nanoparticles was not annihilated and that PBz was arranged on the surface of CeO_2 [31-33]. The average crystallite size was deter-mined using Scherrer's formula and the crystallite size was found to be 8.6 nm.

The XRD patterns of polyurethane, PU-TEOS-PBZ, PU-CeO_2 and PU-TEOS-PBZ@nano-CeO_2 coatings submerged

in 3.5% NaCl for 5 days are displayed in Fig. 3b, individually. The development of foreign materials on the mild steel's surface of PU, PU-TEOS-PBZ, PU-CeO_2 and PU-TEOS-PBZ @nano CeO_2 is observed and examined. The XRD spectrum of polyurethane, PU-TEOS-PBz, PU-CeO_2 and PU-TEOS-PBz @nano CeO_2 coatings is shown in Fig. 3b, which shows the additional peaks are attributable to both FeO and Fe_3O_4. This uncovered that the consumption interaction happened at a rapid rate for polyurethane covered mild steel.

Morphological studies: The surface and bulk morphology of CeO_2 and PBZ@nano CeO_2 with polyurethane nanocomposites were analyzed by SEM with EDX, as shown in Figs. 4a-d and 5a-d, respectively. As can be seen in Fig. 4a-c, CeO_2 nanoparticles as observed by SEM have a typical round shape. The surface modifcation of CeO_2 nanoparticles assisted polybenzoxazine-PU is established by the SEM with EDX examination. SEM/EDX analysis confirms the presence of N, O and Ce in the PBZ@nano-CeO_2 with PU nanocomposites [34-38].

Fig. 5a-d shows the cross-sectional morphologies (SEM and EDX) of mild steel coated with PU, PU-TEOS-PBZ, PU-CeO_2 and PU-TEOS-PBZ/CeO_2 following 5 days of immersion in 3.5% NaCl medium. When PU-TEOS-PBZ/CeO_2 was applied to mild steel, a uniform layer formed, confirming that the CeO_2 nanoparticles did not adhere and a significant scattering was appeared in the coating. Fractures in the mild steel were discovered to exist because of the polyurethane coating. The reduced corrosion on PU coating from PU-TEOS-PBZ, PU-CeO_2 and PU-TEOS-PBZ/CeO_2 nanocomposite coatings was observed and confirmed by reduced required materials. Over time, PU-PBZ/CeO_2 protective coatings are used more and more, but this is a sluggish process since corrugated metal accumulates at the mild steel contact site. The upgraded integrity structures contains Ce, N and O accessible, as determined by the EDX's techniques. The strengthen of reactive metals containing Ce, N at scratch is the main defence for the corrosion inhibition characteristics of PU-PBZ/CeO_2 coated mild steel.

Thermal studies: Usually benzoxazine monomer has intermolecular hydrogen bonding of phenolic hydroxyl group after ring opening polymerization. For this reason, polybenzoxazine gives higher value of glass transition temperature (T_g). Table-1 displays the results for coating weight loss as a function of temperature, with values for 5% weight loss (T_d 5%), 30% weight loss (T_d 30%) and remaining percentage of weight (char yield) at 580-600 ºC. The thermal stability of TEOS-PBZ-PU with CeO_2 nanocomposites coatings is more than polybenzoxazine coating upto 250 ºC and the weight loss of PBZ-PU

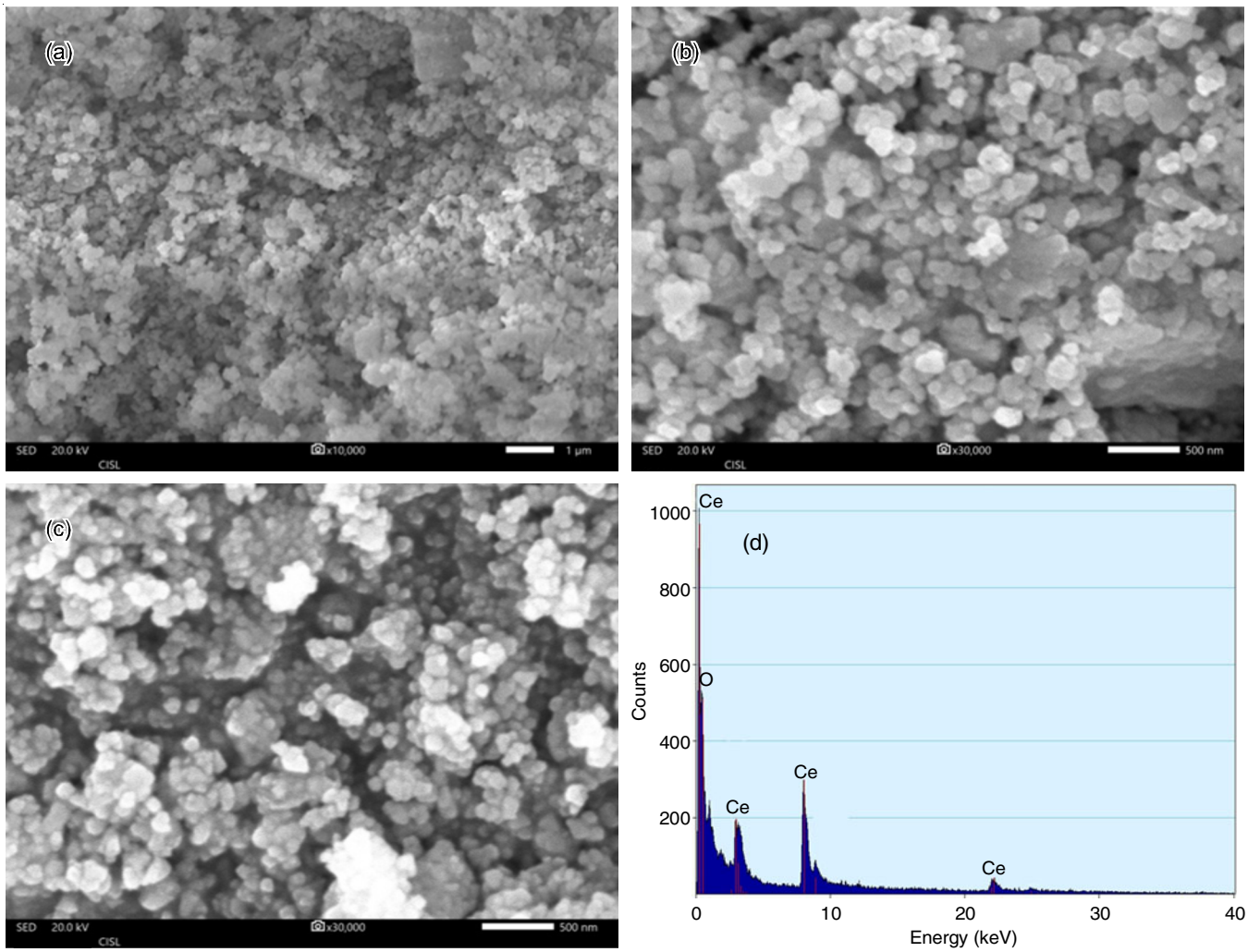

Fig. 4. SEM profile of (a-c) CeO_2 NPs (d) CeO_2 NCs by co-precipitation method

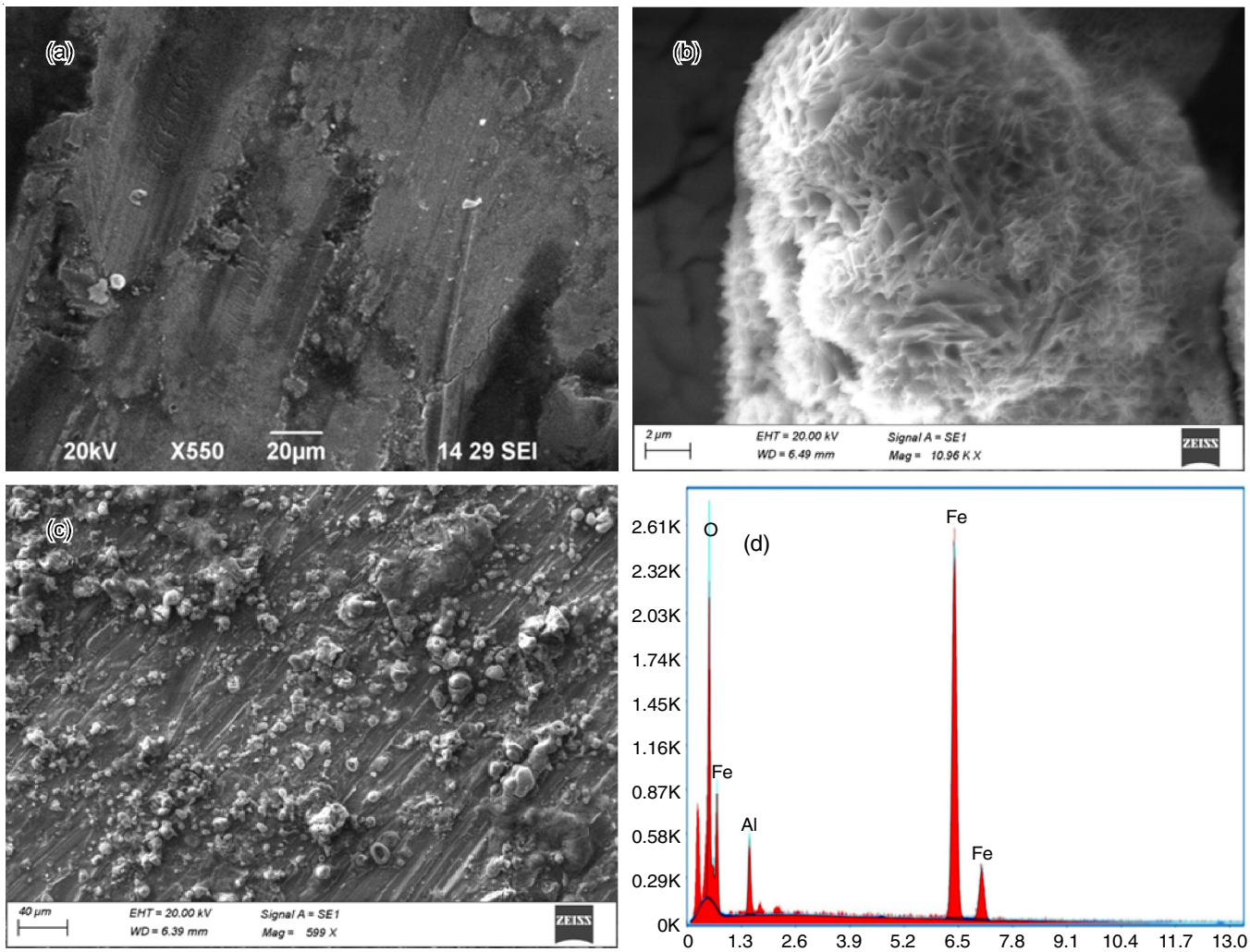

Fig. 5. SEM profile of (a) before coating of polyurethane (b) after coating PU-TEOS-PBz (c) after coating of silane functionalized polybenzoxazine CeO_2 nanocomposites with polyurethane on mild steel in 3.5% NaCl for immersion period 5 day

TABLE-1
TGA DATA OF SILANE FUNCTIONALIZED POLYBENZOXAZINE-PU-CeO_2 NANOCOMPOSITES ON MILD STEEL IN 3.5% NaCl FOR IMMERSION PERIOD 5 DAYS

Coating system	Onset temperature (°C)	Offset temperature (°C)	T_{d5} (°C)	T_{d30} (°C)	T_{HRI}
BZ Monomer	88.38	540	150.24	300.01	115.17
100:60:5% (BZ:PU:Nano)	200.50	560	295.91	412.81	165.04
100:80:5% (BZ:PU:Nano)	210.89	586	278.13	420.16	171.67
100:100:5% (BZ:PU:Nano)	215.09	590	252.72	400.33	169.19

with CeO_2 nanocomposites coatings is less than 10.1% whereas polybenzoxazine coating shows degradation of 14.9% (Fig. 6). These alterations are caused due to the crosslinking density of polyurethane. The crosslinked density of the coating increases as the polyurethane concentration increases.

The thermal stability of coating increases with increasing polyurethane content is evident from Table-1. For this reason, the char yield of silane-functionalized polybenzoxazine@CeO_2 nanocomposites with a polyurethane coating method is lower than that of nanocomposites made with polybenzoxazine alone [39-41]. The following equation is used to calculate the heat resistance index [42-45]:

$$T_{HRI} = 0.49 \times [T_5 + 0.6 \text{ x } (T_{30} - T_5)]$$

DTA analysis: Fig. 7 shows DTA thermograms of silane-functionalized PBz@CeO_2 nanocomposites with polyurethane improved coating at varying molar ratios, with the coating temperature with increasing urethane moiety concentration.

DSC analysis: At 454 ºC, an exothermic peak is displayed on the DSC thermogram of silane-functionalized PBz@CeO_2 nanocomposites with polyurethane as a result of crystallization temperature at 532 ºC and 552 ºC, two exothermic peaks are displayed as a result of the melting temperatures (Fig. 8). These are liable for the ring opening polymerization of TEOS-PBz. As a result of interaction of isocyanate moiety with polybenzoxazine through hydrogen bonding, DSC thermograms of PU-PBz@CeO_2 nanocomposite shows two endothermic peaks at

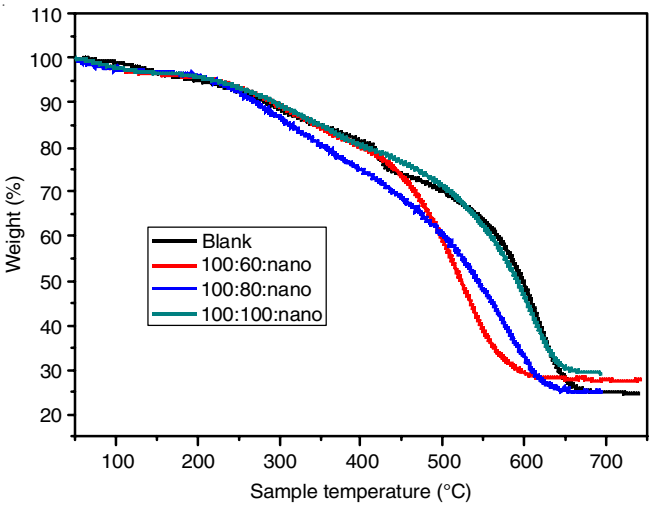

Fig. 6. TGA of benzoxazine monomer and silane functionalized polybenzoxazine CeO_2 NCs with PU at different concentrations

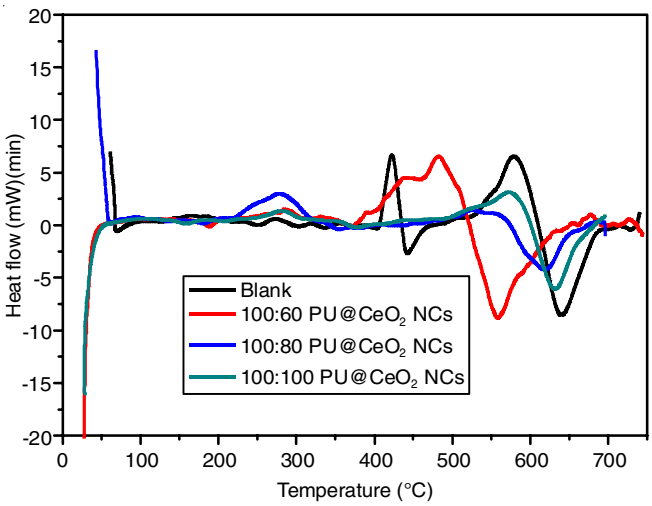

Fig. 7. DTA analysis of silane functionalized polybenzoxazine CeO_2 nanocomposites with Polyurethane at different concentrations on mild steel in 3.5% NaCl for 5 days immersion

458 ºC, 567 ºC for PU:PBz@CeO_2 nanocomposites (100:60:5%), 458 ºC, 574 ºC for PU:PBz@CeO_2 nanocomposites (100:80:5%) and 461 ºC, 575 ºC for PU:PBz@CeO_2 nanocomposites (100:100:5%). Moreover, at 458 ºC and 461 ºC are dependable for the ring opening due to the crosslinking ability of polyurethane at the first exothermic peaks and the second peak at 567, 574 and 575 ºC takes place due to the melting of PU-PBz@CeO_2 nanocomposites. It is not surprising that the polyurethane supported benzoxazine monomer has more heat resistance than

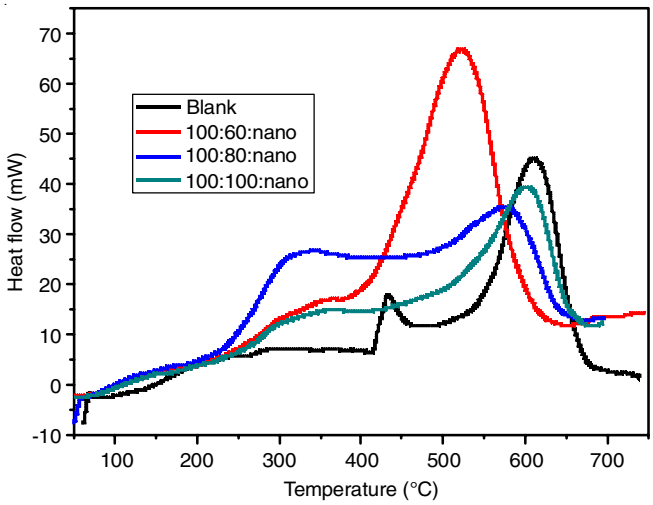

Fig. 8. DSC analysis of silane functionalized polybenzoxazine-PU-CeO_2 NCs at different concentrations on mild steel in 3.5% NaCl for 5 days immersion time

the monomer itself, since both the glass transition temperature and the DSC data were verified.

Electrochemical polarization: The electrochemical polarization curves for bare mild steel and coated mild steel shows the corrosion resistance behaviour of bare mild steel, coated with pure polyurethane and TEOS-PBz-PU@CeO_2 nanocomposites are shown in Fig. 9a. The corrosion parameters such as corrosion potential (E_{corr}), corrosion current (I_{corr}) and anodic/cathodic Tafel slopes (ba and bc) were obtained using the Tafel extrapolation method. The correlation between the silane functionalization of PBz/CeO_2 nanocomposites with polyurethane and the improvement in corrosion protection is evident from the corrosion rates (r_{corr}) data (Table-2). Among all the coated samples, 100% silane functionalized PBz@CeO_2 nanocomposites with polyurethane coated mild steel substrate displayed greater potential shift towards the noble positive corrosion potential (E_{corr}). This indicates that higher amount of ceria with TEOS-Bz nanocomposite coating displayed a better corrosion protection. This could be because large cerium cations rapidly bond with hydroxyl ions, generating a strong double layer on the surface of the mild steel substrate. This retards the charge transfer between the external surroundings and the coated substrates.

The corrosion rate formed for 100% silane functionalized PBz@CeO_2 nanocomposites with polyurethane coated mild steel was 3.851×10^{-2} mm, which is closely 22 times lower than bare mild steel substrate (8.432×10^{-1} mm). The improved

TABLE-2
ELECTROCHEMICAL BEHAVIOUR OF SILANE FUNCTIONALIZED POLYBENZOXAZINE-PU-CeO_2 NANOCOMPOSITES ON MILD STEEL IN 3.5% NaCl FOR IMMERSION PERIOD 5 DAYS

Concentration of samples (polymer:PU:Nano)	Tafel studies				Nyquist plot		
	I_{corr} (uA)	E_{corr} (mV)	Corrosion efficiency (%)	Corrosion Rate	R_{ct} (ohm)	C_{dl} (F)	Inhibition efficiency (%)
Blank	0.042	-491.651	–	488.424	2.825	0.3925	–
100:60:5%	0.042	-515.785	0	488.424	15.32	51.72e-6F	81.39
100:80:5%	0.026	-594.579	38.09	302.350	247.6	52.48e-6F	98.85
100:100:5%	0.002	-368.467	95.23	23.258	1375	7.677e-6F	99.79

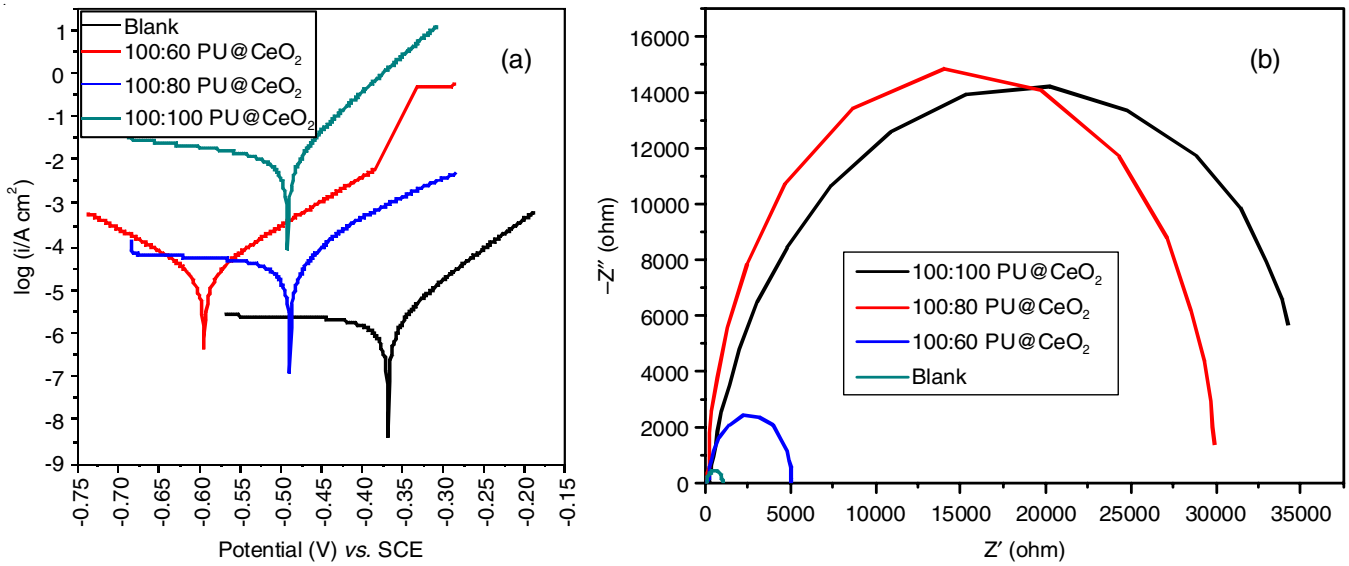

Fig. 9. Electrochemical behaviour of (a) Tafel polarization of CeO_2 NPs and silane functionalized polybenzoxazine-PU-CeO_2 NCs on mild steel in 3.5% NaCl for 5 days (b) Nyquist plot of CeO_2 NPs and silane functionalized polybenzoxazine–PU-CeO_2 NCs on mild steel in 3.5% NaCl for 5 days

corrosion resistance of mild steel in the presence of ceria is attributed to the cathodic site blocking. The precipitation of insoluble cerium hydroxide/ceria at local regions allows the cerium ions to function as cathodic inhibitors at active locations. The electrode impede the cathodic sites, lowering the cathodic current and, as a result, the total corrosion rate.

Fig. 9b shows the Nyquist plot representation/impedance reaction of bare mild steel (MS) substrate, polyurethane resin and silane functionalized PBz/CeO_2 nanocomposites with polyurethane coated MS. At low frequency, the interception with the real axis was attributed to the charge transfer resistance R_{ct} at the corrosion potential. From EIS measurement, the charge transfer resistance (R_{ct}) and double-layer capacitance (C_{dl}) were calculated and the results are presented in Table-2. Compared to blank acrylic resin and mild steel substrate, the R_{ct} values of PU@CeO_2/mild steel and PU/mild steel were extremely high. Better corrosion protection properties are indicated by higher R_{ct} and lower C_{dl} values for 100% PU@CeO_2 nanocomposite coated MS substrates compared to bare substrates.

Micro-hardness testing: A Vickers micro hardness tester was used to calculate the micro-hardness of the condensed specimens. Throughout the duration of the analysis, the loading load ranges from 200 to 263.1 g and the loading time is 11 s (Table-3). As the concentration of polyurethane increased with addition of CeO_2 nanoparticles in the coating will increase the crosslinking ability, due to the absence of hydroxyl group will decrease the empty space.

TABLE-3
MICRO HARDNESS TESTING OF SILANE FUNCTIONALIZED PBZ-PU-CERIUM OXIDE NANOCOMPOSITES ON MILD STEEL IN 3.5% NaCl FOR IMMERSION PERIOD 5 DAYS

Samples	Micro-hardness
Blank	200.65
ST1	224.3
ST2	241.8
ST3	272.1

Gel content: Accurately weighed the cured sample and extracted in xylene for 5 days at room temperature was found as cured coating sample by gel content (Table-4). Then, the cured coating samples were dried in the oven. Gel content of coating was calculated by the following equation:

$$\text{Gel absorption} = \left(\frac{W_a}{W_b}\right)\times 100$$

where W_a and W_b are the weight of cured coating sample after and before the extraction, respectively.

TABLE-4
GEL CONTENT TESTING OF SILANE FUNCTIONALIZED CERIUM OXIDE NANOCOMPOSITES ON MILD STEEL IN 3.5% NaCl FOR IMMERSION PERIOD 5 DAYS

Samples	Gel content
BZ (silyl)	87.11
BZ100:PU60:5%CeO_2	92.31
BZ100:PU80:5%CeO_2	94.82
BZ100:PU100:5%CeO_2	95.15

Water absorption: Water absorption was performed in the cured coating samples as per ASTM D570. The cured coating samples were dried at 80 ºC in a vacuum oven and then immersed in water for 5 days at room temperature. The cured samples were removed from the water, then blotted with tissue papers and weighed. The percentage water absorption was calculated by the following equation:

$$\text{Water absorption} = \left(\frac{W_a - W_b}{W_b}\right)\times 100$$

where W_a and W_a are the weights of the cured sample after and before removal from water absorption. The results in Table-5 show that as coating polyurethane concentration with CeO_2 nanoparticles increases, crosslinking ability increases and simultaneously free space decreases because of the empty hydroxyl

TABLE-5
WATER ABSORPTION ANALYSIS OF SILANE FUNCTIONALIZED CERIUM OXIDE NANOCOMPOSITES ON MILD STEEL IN 3.5% NaCl FOR IMMERSION PERIOD 5 DAYS

Samples	Water absorption
BZ (silyl)	1.15
BZ100:PU60:5%CeO_2	0.87
BZ100:PU80:5%CeO_2	0.72
BZ100:PU100:5%CeO_2	0.63

group. This is evident for the same reason that increasing the percentage of polyurethane with CeO_2 nanoparticles in the coating samples reduces their hygroscopicity.

Conclusion

Nanocomposite coatings for mild steel (MS) in 3.5% NaCl medium were effectively prepared using a co-precipitation method using silane-functionalized polybenzoxazine, CeO_2 and polyurethane. The nanocomposite coatings made of ultra-thin polyurethane and CeO_2 showed an excellent resistance to corrosion. The corrosion protection effectiveness of silane-functionalized polybenzoxazine/CeO_2 improves as the ceria content increases. The mechanical properties were analyzed by using a pull-out adhesion and micro-hardness analyses to determine the level of hardness. The experiments found that polyurethane coated mild steel had greater bonding strength and hardness with the silane functionalized polybenzoxazine/CeO_2 nanocomposites. These results demonstrated that even after prolonged immersion in a corrosive environment, polyurethane coated mild steel embedded with silane functionalized polybenzoxazine, CeO_2 nanocomposites exhibited the highest levels of corrosion resistance. Therefore, the polybenzoxazine/CeO_2 nanocomposites modified with silane functionalized polyurethane matrix with the optimum coatings in industrial applications to extend the lifetime of metals.

CONFLICT OF INTEREST

The authors declare that there is no conflict of interests regarding the publication of this article.

REFERENCES

1. H. Deng, L. Lin, M. Ji, S. Zhang, M. Yang and Q. Fu, *Prog. Polym. Sci.*, **39**, 627 (2014); https://doi.org/10.1016/j.progpolymsci.2013.07.007
2. T. Agag and T. Takeichi, *Polymer*, **52**, 2757 (2011); https://doi.org/10.1016/j.polymer.2011.04.044
3. N.K. Kwon, H. Kim, I.K. Han, T.J. Shin, H.-W. Lee, J. Park and S.Y. Kim, *ACS Macro Lett.*, **7**, 962 (2018); https://doi.org/10.1021/acsmacrolett.8b00475
4. Y. Kuang, L. Zhao, S. Zhang, F. Zhang, M. Dong and S. Xu, *Materials*, **3**, 5220 (2010); https://doi.org/10.3390/ma3125220
5. J.-M. Yeh, S.-J. Liou, C.-Y. Lai, P.-C. Wu and T.-Y. Tsai, *Chem. Mater.*, **13**, 1131 (2001); https://doi.org/10.1021/cm000938r
6. R. Bayan and K. Karak, *Compos. Part A*, **110**, 142 (2018); https://doi.org/10.1016/j.compositesa.2018.04.024
7. S.C. Endres, L.C. Ciacchi and L. Mädler, *J. Aerosol Sci.*, **153**, 105719 (2021); https://doi.org/10.1016/j.jaerosci.2020.105719
8. S.-L. Bee, M.A.A. Abdullah, S.-T. Bee, L.T. Sin and A.R. Rahmat, *Prog. Polym. Sci.*, **85**, 57 (2018); https://doi.org/10.1016/j.progpolymsci.2018.07.003
9. T.D. Dziubla, V.V. Shuvaev, N.K. Hong, B.J. Hawkins, M. Madesh, H. Takano, E. Simone, M.T. Nakada, A. Fisher, S.M. Albelda and V.R. Muzykantov, *Biomaterials*, **29**, 215 (2008); https://doi.org/10.1016/j.biomaterials.2007.09.023
10. C. Garnacho, R. Dhami, E. Simone, J. Leferovich, E.H. Schuchman, T. Dziubla, V. Muzykantov and S. Muro, *J. Pharmacol. Exp. Ther.*, **325**, 400 (2008); https://doi.org/10.1124/jpet.107.133298
11. E.D. Hood, M. Chorny, C.F. Greineder, I. S. Alferiev, R.J. Levy and V.R. Muzykantov, *Biomaterials*, **35**, 3708 (2014); https://doi.org/10.1016/j.biomaterials.2014.01.023
12. K.M. Poole, C.E. Nelson, R.V. Joshi, J.R. Martin, M.K. Gupta, S.C. Haws, T.E. Kavanaugh, M.C. Skala and C.L. Duvall, *Biomaterials*, **41**, 166 (2015); https://doi.org/10.1016/j.biomaterials.2014.11.016
13. E. Hood, E. Simone, P. Wattamwar, T. Dziubla and V. Muzykantov, *Nanomedicine*, **6**, 1257 (2011); https://doi.org/10.2217/nnm.11.92
14. M.K. Gupta, J.R. Martin, T.A. Werfel, T. Shen, J.M. Page and C.L. Duvall, *J. Am. Chem. Soc.*, **136**, 14896 (2014); https://doi.org/10.1021/ja507626y
15. N. Jayakumar, K. Karattu Veedu and N.K. Gopalan, *ACS Appl. Nano Mater.*, **2**, 2689 (2019); https://doi.org/10.1021/acsanm.9b00172
16. Y. Yagci, B. Kiskan and N.N. Ghosh, *J. Polym. Sci. A*, **47**, 5565 (2009); https://doi.org/10.1002/pola.23597
17. S. Rimdusit, S. Tiptipakorn, C. Jubsilp and T. Takeichi, *React. Funct. Polym.*, **73**, 369 (2013); https://doi.org/10.1016/j.reactfunctpolym.2012.04.022
18. Z. Zhang, L. Liu, D. Xu, R. Zhang, H. Shi, S. Luan and J. Yin, *Acta Chim. Sin.*, **80**, 1436 (2022); https://doi.org/10.6023/A21120593
19. L. Qu and Z. Xin, *Langmuir*, **27**, 8365 (2011); https://doi.org/10.1021/la200073v
20. L. Liu, F. Wang, Y. Zhu and H. Qi, *Polymer*, **51**, 5567, (2022); https://doi.org/10.1177/09540083221128295
21. C. Zhou, X. Lu, Z. Xin and J. Liu, *Corros. Sci.*, **70**, 145 (2013); https://doi.org/10.1016/j.corsci.2013.01.023
22. C. Yan, X. Fan, J. Li and S.Z. Shen, *J. Appl. Polym. Sci.*, **120**, 1525 (2011); https://doi.org/10.1002/app.33383
23. C. Zhou, X. Lu, Z. Xin, J. Liu and Y. Zhang, *Corros. Sci.*, **80**, 269 (2014); https://doi.org/10.1016/j.corsci.2013.11.042
24. X. Ning and H. Ishida, *J. Polym. Sci. A Polym. Chem.*, **32**, 1121 (1994); https://doi.org/10.1002/pola.1994.080320614
25. J.A. Macko and H. Ishida, *Polymer*, **42**, 6371 (2001); https://doi.org/10.1016/S0032-3861(01)00055-6
26. R.-C. Lin and S.-W. Kuo, *RSC Adv.*, **8**, 13592 (2018); https://doi.org/10.1039/C8RA00506K
27. X. Yang, S. Fan, Y. Li, Y. Guo, Y. Li, K. Ruan, S. Zhang, J. Zhang, J. Kong and J. Gu, *Compos., Part A Appl. Sci. Manuf.*, **128**, 105670 (2020); https://doi.org/10.1016/j.compositesa.2019.105670
28. M. Mohamad, J.A. Razak, N. Mohamad, S.H. Ahmad, R. Junid and P. Puspitasari, *IOP Conf. Ser.: Mater. Sci. Eng.*, **957**, 012029 (2020); https://doi.org/10.1088/1757-899X/957/1/012029
29. Sudha and Sarojadevi, *High Perform. Polym.*, **28**, 331 (2016); https://doi.org/10.1177/0954008315580822
30. K.S. Kumar and N.V. Jaya, *Asian J. Chem.*, **25**, 6095 (2013); https://doi.org/10.14233/ajchem.2013.14267
31. H. Li, G. Wang, F. Zhang, Y. Cai, Y. Wang and I. Djerdj, *RSC Adv.*, **2**, 12413 (2012); https://doi.org/10.1039/c2ra21590j
32. S.K. Kannan and M. Sundrarajan, *Int. J. Nanosci.*, **13**, 1450018 (2014); https://doi.org/10.1142/S0219581X14500185
33. K. Kalantar-zadeh and B. Fry, *Nanotechnol.-Enabled Sensors*, **211**, 211 (2008); https://doi.org/10.1007/978-0-387-68023-1_5

34. P. Sharma, B. Lochab, D. Kumar and P.K. Roy, *ACS Sustain. Chem. Eng.*, **4**, 1085 (2016); https://doi.org/10.1021/acssuschemeng.5b01153
35. B. Lochab, M. Monisha, N. Amarnath, P. Sharma, S. Mukherjee and H. Ishida, *Polymers*, **13**, 1260 (2021); https://doi.org/10.3390/polym13081260
36. M.S. Pujar, S.M. Hunagund, V.R. Desai and A.H. Sidarai, *Bull. Mater. Sci.*, **43**, 24 (2018); https://doi.org/10.5185/amp.2018/019
37. J. Hou, L. Huo, C. He, C. Yang and Y. Li, *Macromolecules*, **39**, 594 (2006); https://doi.org/10.1021/ma051883n
38. C. Aouf, H. Nouailhas, M. Fache, S. Caillol, B. Boutevin and H. Fulcrand, *Eur. Polym. J.*, **49**, 1185 (2013); https://doi.org/10.1016/j.eurpolymj.2012.11.025
39. S. Pirstpindvong, W. Tanthapanichakoon, S. Damrongsakkul and S. Rimdusit, *Polym. Eng. Sci.*, **45**, 288 (2005); https://doi.org/10.1002/pen.20273
40. S.D. Silbert, E.M. Serum, J. LaScala, M.P. Sibi and D.C. Webster, *ACS Sustain. Chem. Eng.*, **7**, 19621 (2019); https://doi.org/10.1021/acssuschemeng.9b04713
41. X. Luo, F. Gao, F. Chen, Q. Cheng, J. Zhao, X. Wei, C. Lin, J. Zhong and L. Shen, *RSC Adv.*, **10**, 15881 (2020); https://doi.org/10.1039/D0RA01279C
42. M.S. Pujar, S.M. Hunagund, V.R. Desai, S. Patil and A.H. Sidarai, *AIP Conf. Proc.*, **1942**, 050026 (2018); https://doi.org/10.1063/1.5028657
43. J. Chen, M. Zeng, Z. Feng, T. Pang, Y. Huang and Q. Xu, *ACS Appl. Polym. Mater.*, **1**, 625 (2019); https://doi.org/10.1021/acsapm.8b00083
44. M. Ohara, K. Yoshimoto, T. Kawauchi and T. Takeichi, *Polymer*, **202**, 122668 (2020); https://doi.org/10.1016/j.polymer.2020.122668
45. P. Sharma, P. Dutta and L. Nebhani, *Polymer*, **184**, 121905 (2019); https://doi.org/10.1016/j.polymer.2019.121905